JPE 5-4-6

Induction Generator Using PWM Converter and Its Small-Scale Power Applications to Variable-Speed Renewable-Energy Generation

Tarek Ahmed†, Katsumi Nishida** and Mutsuo Nakaoka*

†*The Graduate School of Science and Engineering, Yamaguchi University, Yamaguchi, Japan
**Ube National College of Technology, Yamaguchi, Japan

ABSTRACT

This paper describes a simple control structure and power conditioning system for an indirect vector controlled stand-alone induction generator (IG) used to operate under variable speed. The required reactive power for the IG system is supplied by means of a capacitor bank and a voltage-source PWM converter. Using a capacitor bank to transfer the reactive power to the IG under the rated speed and no-load conditions starts the IG operation and reduces the PWM converter size. The vector control structure for the variable speed IG power conditioning system compensates for changes in the electrical three-phase and DC loads while considering the magnetizing curve of the IG. The vector control structure is developed to regulate the DC link voltage of the PWM converter and the IG output voltage. The experimental and simulated performance results of the IG power conditioning system at various speeds and loads are given and show that this proposed scheme can be used efficiently for a variable speed, wind energy conversion system.

Keywords: Induction Generator, Vector Control, AC and DC Small-Scale Power Applications, PWM Converter

1. Introduction

A squirrel-cage induction generator (IG), with its lower maintenance demands and simplified controls, appears to be an effective solution for small hydro and wind power plants[1]. For its simplicity, vitality, and small size per generated kW, the IG is favored for such applications[2-4]. Recently there is an increase in global use of induction machines in wind power generation, especially to supply electric power in remote areas where utility lines are uneconomical to install due to terrain, the right-of-way difficulties or the environment concerns. Even without these constraints, building new transmission lines is expensive. For remote villages farther than two miles from the nearest power transmission line, a stand-alone wind system could be more economical.

One of the major problems with the stand-alone IG is its inherently poor voltage regulation with speed or load variation. Therefore, it becomes necessary to have an appropriate voltage regulation scheme. There are many schemes that have been proposed[5-10]. Some of these proposals use inverters and field-orientation algorithms to excite and control the three-phase IG. That enables a stiff voltage regulation and high efficiency[5-8]. As a drawback, there is a need for a battery, which acts as a voltage source to the inverter and also supplies reactive power to the

Manuscript received July 7, 2005; revised September, 5, 2005
†Corresponding Author: tarek@pe-news1.eee.yamagychi-u.ac.jp
Tel: +81-836-85-9472, Fax: +81-836-85-9401, Yamaguchi Univ.
*The Graduate School of Sci. and Eng., Yamaguchi Univ.
**Ube National College of Technology

induction machine. Therefore, the inverter has to be designed for the rated power and the battery life will decrease due to high ripple currents if filter capacitors are not used. As a result this scheme is not cost effective for renewable power generation. There is also an additional decoupling compensation that should be applied for vector control in the stator flux orientation.

Due to the increase of the electrical load demand for stand-alone applications, an induction-machine-based stand-alone power generation scheme with a diode bridge rectifier and a PWM-VSI that uses the rotor field orientation has been proposed to control the output voltage of the diode bridge rectifier[9]. However, there is a serious voltage harmonics problem with this proposed power system.

Based on the instantaneous reactive power theory, using a capacitor bank and an inverter simultaneously without any mechanical position sensor in the induction machine rotor has been proposed [10]. There are many voltage and current sensors that have been used to achieve the wanted result of the proposed strategy, but they also produce a poor ac voltage regulation especially with a low speed.

In this paper, the indirect vector or rotor field-oriented control of an IG is presented, yielding high dynamic performances. A hybrid excitation unit, consisting of a capacitor bank and a PWM converter, is used for the IG loaded with three-phase loads and DC loads. This is a more reliable and simple method of IG voltage control and it can start and generate its output voltage and reduce the rating of the PWM converter. The capacitor bank and converter can supply the required reactive power to regulate both the IG output and DC link voltages.

2. Induction Generator Control

In Fig.1, the IG is controlled in a synchronously rotating d-q axis frame, with the d-axis oriented along the rotor-flux vector position. In this approach, a decoupled control between the reactive and active currents is obtained. The stator flux linkages in terms of the stator reactive and active currents are varied to control the IG output voltage and the DC-link voltage under the conditions of variable speeds and different load types. The PWM converter provides the actuation and the control requires the measurement of the stator currents of the IG and the AC-side currents of the converter. In general, subsystem A of Fig.1 is used for the calculation of the rotor-flux vector position. Subsystem B is proposed for the line-to-line voltage regulation and for calculating the *d*-axis reference current. Subsystem C is presented for the stator *d-q* axis IG voltages calculator. Subsystem D is used for the DC voltage and the *d-q* axis current controllers with the decoupled control system.

Under the rotor field-oriented control of the IG, the relationship between the torque and the *d-q* axis voltages, currents and fluxes may be written as [1],

$$\lambda_r = \lambda_{dr} = -\tau_r \frac{d}{dt}\lambda_{dr} + L_m i_{ds} \quad , \quad \lambda_{qr} = 0 \tag{1}$$

$$\lambda_{ds} = \frac{L_m}{L_r}\lambda_{dr} + \sigma L_s i_{ds} \, , \quad \lambda_{qs} = \sigma L_s i_{qs} \tag{2}$$

$$i_{qr} = -\frac{L_m}{L_r} i_{qs} \, , \quad i_{dr} = \frac{\lambda_{dr} - L_m i_{ds}}{L_r} \tag{3}$$

$$i_{ms} = i_{ds}\sqrt{1+(1-\sigma)^2\left(\frac{i_{qs}}{i_{ds}}\right)^2} \, , \quad \sigma = 1 - \frac{L_m^2}{L_s L_r} \tag{4}$$

$$v_{ds} = r_s i_{ds} + \sigma L_s \frac{di_{ds}}{dt} - \omega\sigma L_s i_{qs} + \frac{1}{\tau_r}\left(-\frac{L_m}{L_r}\lambda_{dr} + \frac{L_m^2}{L_r} i_{ds}\right) \tag{5}$$

$$v_{qs} = r_s i_{qs} + \sigma L_s \frac{di_{qs}}{dt} + \omega\sigma L_s i_{ds} + \omega\frac{L_m}{L_r}\lambda_{dr} \tag{6}$$

$$T_e = -\frac{3P}{4}\left(\omega L_m i_{ms} i_{qs}\right), \quad \omega_{sr} = \left(\frac{1}{\tau_r}\right)\left(\frac{L_m}{\lambda_{dr}}\right) i_{qs} \tag{7}$$

When τ_r (L_r / r_r) is the rotor time constant of the IG, the equivalent-circuit parameters, L_{ls}=L_{lr}=3.7 mH, r_s=0.6 Ω, and r_r=0.6 Ω, are obtained by the experimental measurements on a laboratory model 5-kW, 220 V, 18.0 A 60 Hz, 4-poles, squirrel-cage induction machine.

Since the stator of the IG is connected to an isolated load, the stator magnetizing current i_{ms} cannot be considered constant. The relationship between the magnetizing inductance L_m and the magnetizing phase current ($i_{ms}/\sqrt{2}$) is obtained experimentally as depicted in Fig.2. The value of the magnetizing inductance L_m is a nonlinear function of the magnetizing phase current and may be expressed as follows

$$L_m = \frac{1}{120\pi}\begin{cases} -0.013i_m^4 + 0.33i_m^3 & 0 < i_m \le 7.4 \\ -2.8i_m^2 + 6.4i_m + 30.7 & \\ -1.1i_m + 27 & 7.4 < i_m \le 15.6 \end{cases} \quad (8)$$

The accuracy of the rotor flux angle is critical in the rotor vector control where the calculation of currents like the *d-q* axis currents of the IG, i_{ds} and i_{qs} in the synchronous frame are determined by the electrical rotor flux angle θ_e. Therefore, this vector control method relies on knowledge of magnetizing inductance L_m where the real values of which may change as operating conditions change. The rotor-flux vector position θ_e is found by calculating the magnitude of the rotor flux in steady-state is, $\lambda_{dr}^* = L_m i_{ms} = L_m i_{ds}^*$. Quantities that are commanded or estimated in drive control are denoted by an asterisk (*).

$$\theta_e^* = \int \left(\frac{L_m i_{qs}^*}{\tau_r \lambda_{dr}^*} + \omega_r \right) dt \quad (9)$$

In simulation, the block diagram of the rotor-flux vector position θ_e is depicted in Fig.3 while the integral in (9) is solved in the experiment by using a digital filter with a cutoff frequency of 0.5 Hz that eliminates DC offset.

2.1 d-q axis voltages of an induction generator

Since the stator of the IG is connected to a fixed capacitor, there is no need to measure its output voltages as they are calculated in the designed simulation program. Fig.4 shows the schematic diagram used for calculation of the stator *d-q* axis IG voltages v_{qs} and v_{ds} and line-to-line voltage v_l. Both require the measurement of the IG stator currents and the AC-side currents of the PWM converter.

The *d-q* axis voltage-current equations of the fixed capacitor may be written as follows [1]:

$$\begin{aligned} i_{qf} &= C_{ac}\frac{dv_{qs}}{dt} + \omega_s C_{ac} v_{ds} \\ i_{df} &= C_{ac}\frac{dv_{ds}}{dt} - \omega_s C_{ac} v_{qs} \end{aligned} \quad (10)$$

where C_{ac} is the fixed excitation capacitance. $i_{qf} = -(i_{qs} + i_{qi} + i_{ql})$ and $i_{df} = -(i_{ds} + i_{di} + i_{dl})$, are respectively the *q*-axis

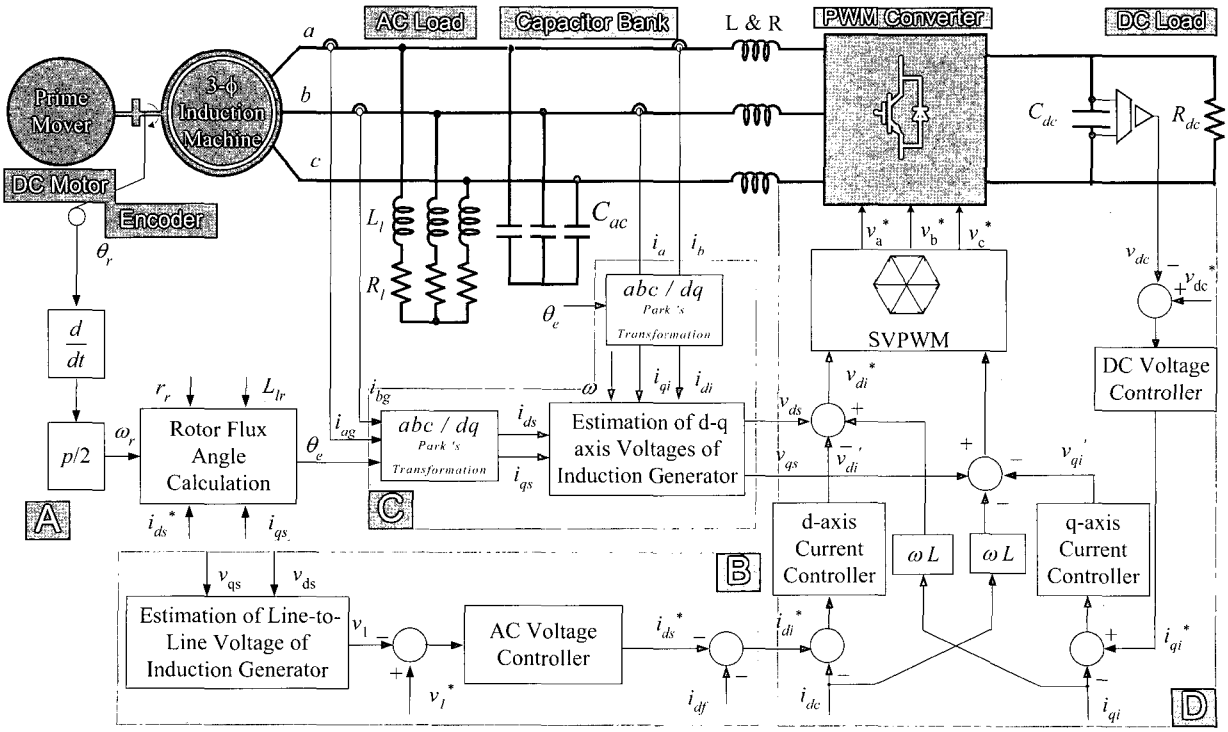

Fig. 1 Induction generator for small-scale AC and DC power applications

and d-axis components of the fixed capacitor current. i_{ql} and i_{dl} are the d-q axis currents of an inductive load (R_l, L_l) connected across the IG's stator terminals. i_{qi} and i_{di} are d-q axis currents of the PWM converter.

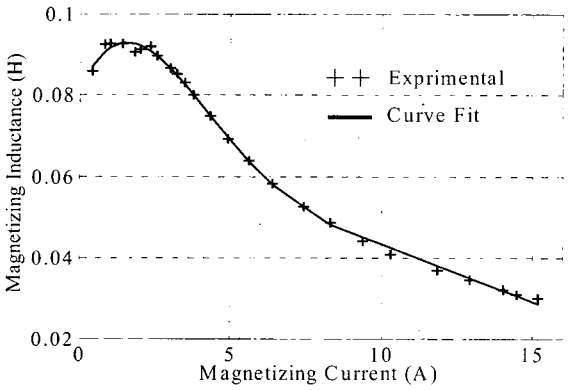

Fig. 2 Magnetizing inductance versus magnetizing current

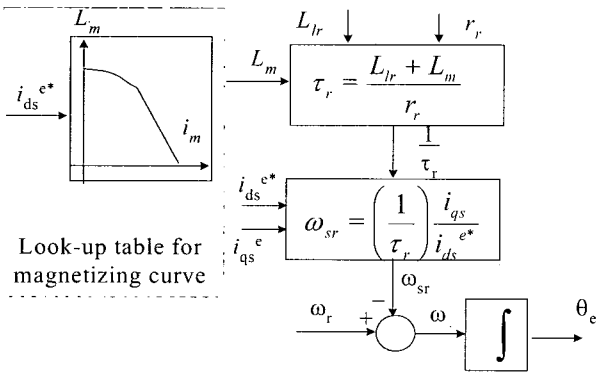

Fig. 3 Block diagram for rotor flux angle calculation

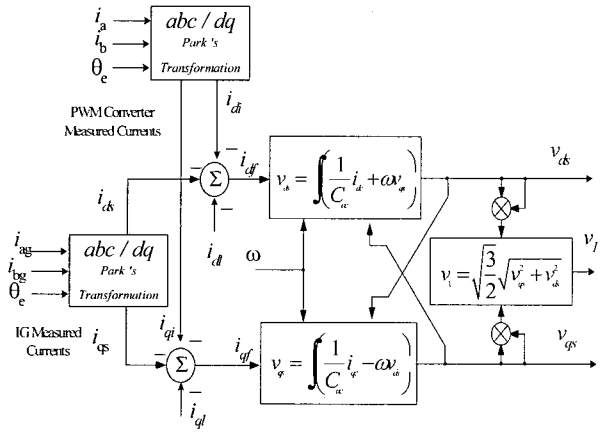

Fig. 4 Schematic block diagram for calculating d-q axis IG voltages

2.2 Design of an IG output voltage loop

The block diagram of the PI controller of the IG output voltage control loop is shown in Fig.5. This simplified model is obtained from (1) and (6) while assuming v^*_l ($v^*_l = \left(\sqrt{3/2}\right)\sqrt{v^2_{qs}+v^2_{ds}} \cong \left(\sqrt{3/2}\right)v_{qs}$) and the inner loops of the d-q axis currents are ideal. The transfer function of the q-axis voltage to the d-axis reference current of the IG is as follows:

$$\frac{v_{qs}(s)}{i^*_{ds}(s)} = \frac{\omega L^2_m}{L_r(1+\tau_r s)} \tag{11}$$

Using the nominal drive model, the transfer function of the current response to the command input of Fig.5 is below:

$$\frac{v_l(s)}{v^*_l(s)} = \sqrt{\frac{3}{2}}\frac{\omega L^2_m k_{ii}}{\tau_r L_r}\frac{(T_i s+1)}{\left(s^2+2\zeta_i\omega_{ni}s+\omega^2_{ni}\right)} \tag{12}$$

The parameters of the PI controller are given below.

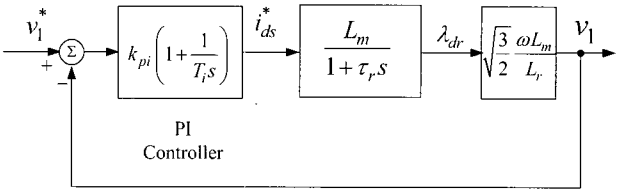

Fig. 5 IG-output voltage control loop

$$k_{pi} = \sqrt{\frac{2}{3}}\frac{L_r}{\omega L^2_m}\left(2\xi_i\tau_r\omega_{ni}-1\right),\quad T_i = \frac{k_{pi}}{k_{ii}} = \frac{\left(2\xi_i\tau_r\omega_{ni}-1\right)}{\tau_r\omega^2_{ni}}$$

With damping ratio $\xi = \sqrt{2}/2$, the unit step response of equation (12) is

$$v_l(t) = 1 - \frac{1}{\sqrt{1-\xi_i^2}}e^{-\xi_i\omega_{ni}t}\left[\left(-\xi_i+\frac{1}{\tau_r\omega_{ni}}\right)\sin\left(\omega_{ni}\sqrt{1-\xi_i^2}\,t\right) + \sqrt{1-\xi_i^2}\cos\left(\omega_{ni}\sqrt{1-\xi_i^2}\,t\right)\right] \tag{13}$$

From (13), the desired tracking specifications can be completely achieved by using the simple PI controller while specifying the response time t_{re}, and solving the above nonlinear equation to obtain ω_{ni}. Using the parameters, τ_r =0.113 s and L_m = 0.0661 H, at the

full-load 5 kW and rated speed ω = 377 rad.s^{-1} with setting t_{re} to 0.07 s, the parameters of the PI controller are, k_{Pi} =0.0611 AV^{-1}, k_{ii}= 1.26 A(Vs)$^{-1}$and T_i = 0.0485 s where ω_{ni} = 20 rad.s^{-1}.

2.3 Design of capacitor bank

Based upon the whole reactive-current needed to generate the rated voltage under the no-load and rated speed conditions, the capacitor bank can be simply designed for the stand-alone IG capacitive excitation. Therefore, the stator reactive current is given by;

$$i_{ds} = \omega C_{ac} v_{qs} \tag{14}$$

The fixed capacitance may be defined with substituting, the stator voltage v_{qs} of (11) in the steady-state to (14) as,

$$C_{ac} = \frac{1}{\omega^2 L_m} \tag{15}$$

From (15) and the magnetizing curve depicted in Fig.2, the minimum capacitance; C_{min} required for building-up the stand-alone IG voltage at the rated speed n =1800 r/min, can be estimated with L_m = L_{unsm} = 0.9 H where L_{unsm} is the unsaturated magnetizing inductance. Therefore, the required excitation capacitance for the IG from the no-load to the full-load under the rated speed condition is between C_{min} ≅ 80 μ F to 230 μ F. Fig.6 shows the calculated excitation capacitance against the line-to-line input voltage of the induction machine (IM) at no-load and different speeds (n). A 150 μ F capacitor, which is available in the laboratory, fits the excitation requirement of the IG at no-load.

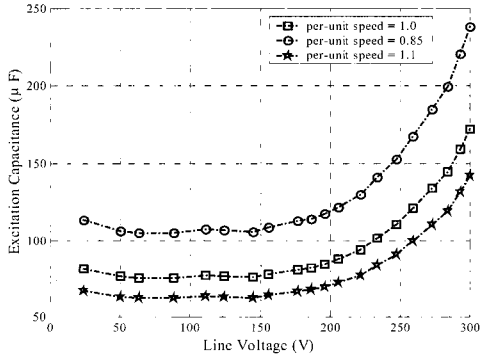

Fig. 6 shows the excitation capacitance against line voltage of IM at no-load

3. PWM Converter Control

The objectives of the PWM converter are mainly to keep both the DC-link and IG terminal voltages constant regardless of the magnitude of the load power or the prime mover speed. A vector-control approach is used with a reference frame oriented along the rotor flux linkage vector position. This enables independent control of the active and reactive current flowing between the AC-side of the converter and the IG connected to a fixed excitation capacitor where the quadrature-axis current used to regulate the DC-link voltage and the direct-axis current component. They are used to regulate the IG terminal voltage scheme through the controlled reactive power of the converter. From Fig.1, a state-space modeling of the PWM converter is given by the voltage balance across the inductors in the d-q reference frame rotating at the angular frequency ω of the IG-output voltage and the power balance between the AC input and the DC output of the PWM converter.

$$\frac{d}{dt}\begin{bmatrix} i_{qi} \\ i_{di} \\ v_{dc} \end{bmatrix} = \begin{bmatrix} -\frac{R}{L} i_{qi} - \omega i_{di} - \frac{1}{L} v_{qi} \\ -\frac{R}{L} i_{di} + \omega i_{qi} - \frac{1}{L} v_{di} \\ \frac{3}{2C_{dc} v_{dc}} (v_{di} i_{di} + v_{qi} i_{qi}) \end{bmatrix} + \begin{bmatrix} \frac{1}{L} v_{qs} \\ \frac{1}{L} v_{ds} \\ -\frac{i_{dcl}}{C_{dc}} \end{bmatrix} \tag{16}$$

Here L and R are the line inductance and resistance, respectively. v_{dc} and i_{dcl} are the DC output voltage and DC load current respectively. From (16), the converter d-q axis currents i_{di} and i_{qi} can be controlled by the control variables v_{di} and v_{qi}. However, the controller is intricate because of a coupling system. For example, a change in v_{di} results in variations on i_{di} , i_{qi} and v_{dc}. Using the controller presented in (17), decoupling between d-q axis currents is achieved with the input variables v'_{qs} and v'_{ds}

$$\begin{aligned} v'_{qs} &= v_{qs} - v_{qi} - \omega L i_{di} \\ v'_{ds} &= v_{ds} - v_{di} + \omega L i_{qi} \end{aligned} \tag{17}$$

The decoupled system state-space model can be presented in the following way:

$$\frac{d}{dt}\begin{bmatrix} i_{qi} \\ i_{di} \end{bmatrix} = \begin{bmatrix} -\frac{R}{L} & 0 \\ 0 & -\frac{R}{L} \end{bmatrix}\begin{bmatrix} i_{qi} \\ i_{di} \end{bmatrix} + \begin{bmatrix} \frac{1}{L} & 0 \\ 0 & \frac{1}{L} \end{bmatrix}\begin{bmatrix} v'_{qi} \\ v'_{di} \end{bmatrix} \tag{18}$$

$$\frac{d}{dt}v_{dc} = \frac{3\left(v_{ds} - v'_{di}\right)}{2C_{dc}v_{dc}}i_{di} + \frac{3\left(v_{qs} - v'_{qi}\right)}{2C_{dc}v_{dc}}i_{qi} - \frac{i_{dcl}}{C_{dc}}$$

It is possible to independently control the *d-q* axis components of the converter currents i_{qi} and i_{di} by v'_{qs} and v'_{ds} respectively. From (18), it is easier to synthesize a required current controller by using (19).

$$F(s) = \frac{i_{di}(s)}{v'_{di}(s)} = \frac{i_{qi}(s)}{v'_{qi}(s)} = \frac{1}{Ls + R} \tag{19}$$

The i_{qi} and i_{di} errors are processed by the PI controller to give v'_{qi} and v'_{di} respectively. To ensure good tracking of these currents, compensation terms are added to v'_{qi} and v'_{di} to obtain the reference voltages v^*_{qi} and v^*_{di} according to (20).

$$\begin{aligned} v^*_{qi} &= -v'_{qi} + \left(-\omega L i_{di} + v_{qs}\right) \\ v^*_{di} &= -v'_{di} + \left(\omega L i_{qi} + v_{ds}\right) \end{aligned} \tag{20}$$

The terms in brackets in (20) constitute voltage-compensation terms. However, these terms are obtained from (5) and (6) in case there is no need for a capacitor bank. The dynamic model of the complete voltage controller depicted in Fig.7 is obtained from the block diagram of the decoupled model in (18) with the models of the *d-q* axis currents and DC voltage controllers.

3.1 Design of current control-loops

The design of the *d-q* axis current controllers may be carried out in a continuous time domain as illustrated in Fig.7. The transfer function of the current response to the command input of Fig.7 can be expressed in the following way:

$$\frac{i_{di}}{i^*_{di}} = \frac{i_{qi}}{i^*_{qi}} = \frac{k_{ic}}{L}\frac{\left(T_c s + 1\right)}{\left(s^2 + 2\zeta_c \omega_{nc} s + \omega_{nc}^2\right)} \tag{21}$$

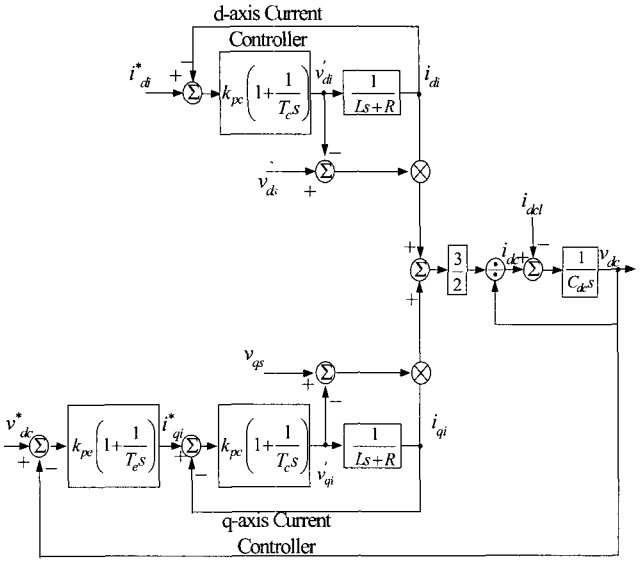

Fig. 7 Model of complete controllers for a PWM converter

From (21) and Fig.7, are defined as the controller parameters k_{pc} and k_{ic} are defined as,

$$k_{pc} = R\left(2\tau_c \xi_c \omega_{nc} - 1\right),\ T_c = \frac{k_{pc}}{k_{ic}} = \frac{2\tau_c \xi \omega_n - 1}{\tau_c \omega_n^2},\ \tau_c = \frac{L}{R}$$

Owing to the existance of zero, the overshoot in the step response of (21) exists. The low overshoot value and fast response are the design criteria. Setting the damping ratio $\xi_c = \sqrt{2}/2$, yields (22) where ω_{nc} depends on t_{re},

$$i(t) = 1 - \frac{1}{\sqrt{1-\xi_c^2}}e^{-\xi_c \omega_{nc} t}\left[\begin{array}{l} \left(-\xi_c + \frac{1}{\tau_c \omega_{nc}}\right)\sin\left(\omega_{nc}\sqrt{1-\xi_c^2}\,t\right) \\ +\sqrt{1-\xi_c^2}\cos\left(\omega_{nc}\sqrt{1-\xi_c^2}\,t\right) \end{array}\right] \tag{22}$$

A maximum value of a nominal closed-loop natural frequency $\omega_{nc} = 140$ rad.s^{-1}is chosen using a simulation program at t_{re} = 0.007 s. For the inductors used, R = 0.1 Ω, L= 6 m H and τ_c =0.06 s, a design for a nominal closed-loop natural frequency $\omega_{nc} = 140$ rad.s^{-1} can be obtained using the PI controller, 1.088(1+117.6/s).

3.2 DC–link voltage loop design

The closed-loop block diagram of the DC-link voltage controller is shown in Fig.7 and it is assumed that the inner i_{qi} loop is ideal. To synthesize the DC voltage controller, a simplified model must be used while

neglecting the dependency of the *d-q* axis currents i_{qi} and i_{di} on the coupled input variables v_{di} and v_{qi}. Then the simplified model of the DC–link voltage loop is depicted in Fig. 8. Assuming that v_{di} is zero, the DC–link voltage can then be controlled acting upon i_{qi} and the transfer function of the PWM converter becomes the following:

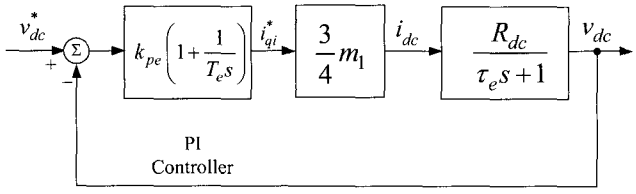

Fig. 8 Simplified DC-link voltage control loop

$$\frac{v_{dc}(s)}{i_{qi}(s)} = \frac{3m_1 R_{dc}}{4(\tau_e s+1)}, \quad \tau_e = R_{dc}C_{dc} \tag{23}$$

Here m_1 is the modulation index. The standard classical design is appropriate. The transfer function is expressed as follows:

$$\frac{v_{dc}}{v_{dc}^*} = \frac{3m_1 k_{ie}}{4C_{dc}} \frac{T_e s+1}{\left(s^2+2\zeta_e\omega_{ne}s+\omega_{ne}^2\right)} \tag{24}$$

For a required voltage response ω_{ne} and $\xi_e = \sqrt{2}/2$, are given by the controller parameters.

$$k_{pe} = \frac{4}{3m_1 R_{dc}}\left(2\xi_e\tau_e\omega_{ne}-1\right), \quad T_e = \frac{k_{pe}}{k_{ie}} = \frac{2\tau_e\xi_e\omega_{ne}-1}{\tau_e\omega_{ne}^2}$$

The unit step response of (24) is as follows:

$$v_{dc}(t) = 1 - \frac{1}{\sqrt{1-\xi_e^2}} e^{-\xi_e\omega_{ne}t}\left[\left(-\xi_e+\frac{1}{\tau_e\omega_{ne}}\right)\sin\left(\omega_{ne}\sqrt{1-\xi_e^2}\,t\right) + \sqrt{1-\xi_e^2}\cos\left(\omega_{ne}\sqrt{1-\xi_e^2}\,t\right)\right] \tag{25}$$

This controller can be used with higher values of ω_{ne}. However, a maximum limit must be imposed because very high values of ω_{ne} also cause oscillations in the system. A maximum value of $\omega_{ne} = 41.20$ rad s^{-1} is chosen using a simulation program at $t_{ri} = 0.03$ s. With $V_{dc} = 350$ V, $m_1 = 0.8284$ (for $V_l = 220$V), $C_{dc} = 3.9$m F, $R_{dc} = 24.5\ \Omega$ and, $\tau_r = 0.096$ s, a controller of 0.27(1+8.874/s) can be shown to give a nominal closed-loop natural frequency of 41.2 rad.s^{-1}.

4. Measured and Simulated Results

4.1 Problems of IG without Voltage Regulation System

One of the serious problems with the IG is its poor voltage regulation. Fig. 9 shows the measured results of the self-excited IG (SEIG) with a 150 μF excitation capacitance and isolated three-phase load. The output power has been increased from no-load to 0.57 kW, with 1600-r/min. The line voltage of the IG has been dramatically decreased from 220 V to 130 V. It was also recognized during the experimental works that the output voltage of the IG will collapse directly with a slight increase of load power. This means that the maximum power that can be supplied from the stand-alone IG without voltage regulation is very small as compared with the rated power of the IG (10 % of the IG rated power). Fig.10 illustrates the simulated and experimental results of the steady-state line-to-line voltage. The speed of the prime mover (in this case a DC motor) is used against the output power of the IG with resistive load variations. Fig.10 proves the maximum power, which can be obtained from the IG with a stable operation and a 150 μF, is about 0.57 kW. The speed slightly changes while increasing the load power due to the electrical loading increase on the IG terminals. Therefore, the frequency variations can be easily recognized due to both the speed and the resistive load changes.

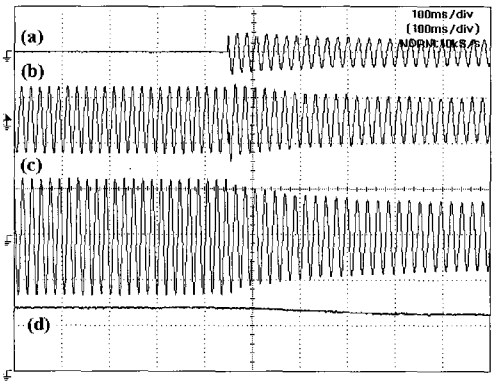

(a) Load current; (12.5 A/ div), (b) IG current; (12.5 A/ div), (c) IG line voltage; (250 V/ div), (d) Speed; (1100 (r/min)/ div)

Fig. 9 Experimental results of IG with capacitor bank

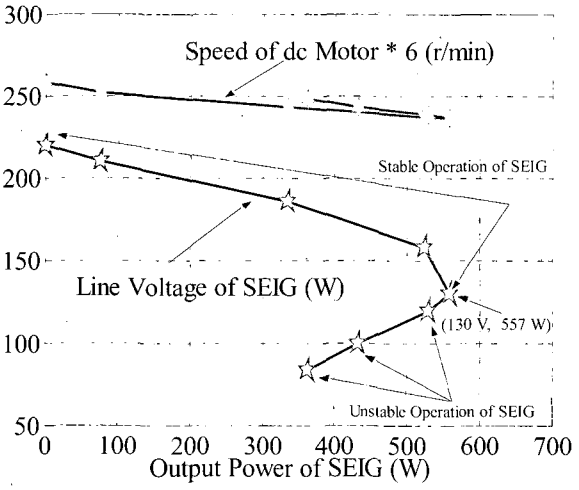

Fig. 10 Steady-state line voltage of IG and speed against resistive load power

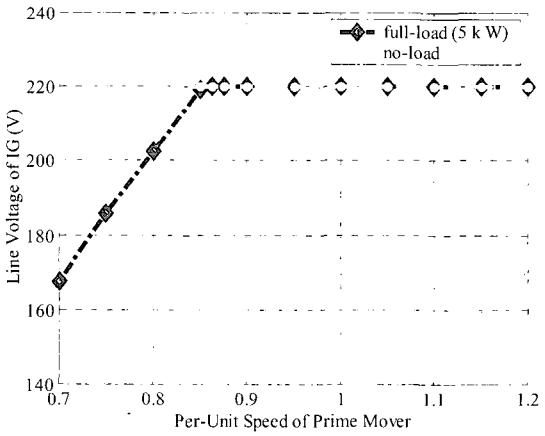

Fig. 11 Line voltage of IG versus per-unit speed of prime mover

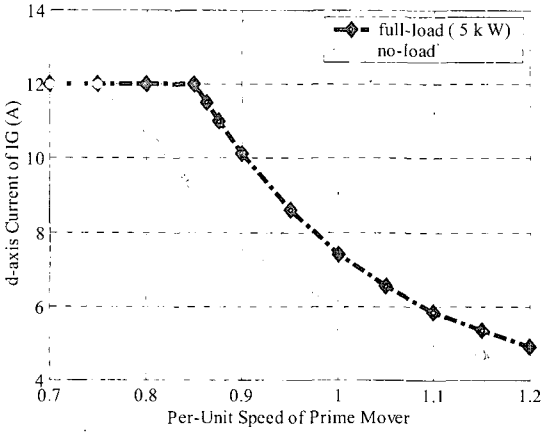

Fig. 12 IG reactive current versus per-unit speed of prime mover

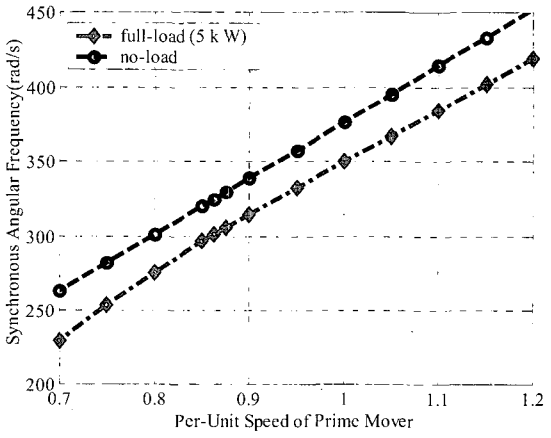

Fig. 13 Synchronous angular frequency versus per-unit rotor speed

4.2 IG Voltage Regulation Scheme with Speed Variations

The Matlab/Simulink environments have been used to design the dynamic model of the proposed IG power conditioning system shown in Fig.1 under various disturbances. In Figs. 11–15, the steady-state results of the IG system are depicted with the DC load stepped from no-load to full-load (Pout = 5 kW) conditions within a per-unit speed range from 0.7 to 1.2 where the DC-link voltage is regulated to a constant voltage of V_{dc}=350 V. Fig. 11 shows the IG line voltage with the prime mover speed. The line-to-line voltage of the IG could not be regulated to the reference voltage of 220 V at low speeds where Pout = 5 kW due to the limitation of the rated stator reactive current (i_{ds}=12 A) and a voltage drop in the IG resistances and leakage inductances, caused by the active current, i_{qs}. However, the line-to-line voltage regulation can still be achieved at no-load. The IG stator reactive current against the prime mover speed is depicted in Fig. 12. The stator reactive current reaches its rated value in an attempt to regulate the stator voltage at the low-speed range. For the high-speed range, the stator reactive current is below the rated value, allowing the controller to achieve IG voltage regulation. The obvious effect of increasing the DC load power and the prime mover speed on the synchronous angular frequency of the IG power conditioning system is depicted in Fig.13. As shown in Fig.14, the per-phase reactive current of the capacitor

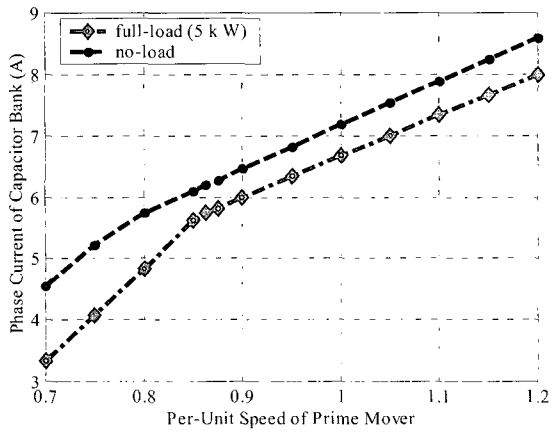

Fig. 14 Phase current of capacitor bank versus per-unit rotor speed

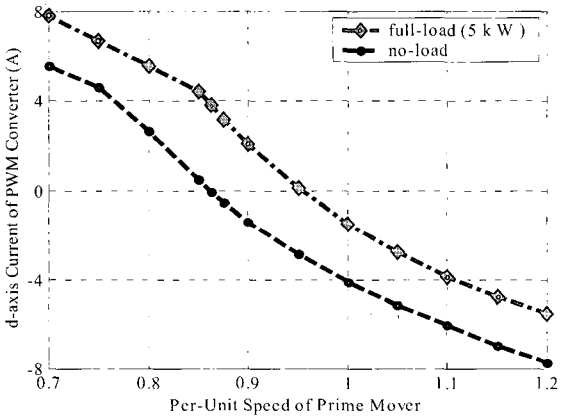

Fig. 15 Reactive current of converter versus per-unit rotor speed

bank depends on the regulated stator voltage and frequency. Therefore, any voltage drop due to the active current has to be compensated by the PWM converter reactive current. Fig.15 shows the reactive current of the PWM converter versus the rotor speed. At lower speeds than 0.95 per-unit, the reactive current supplied from capacitor bank with C = 150 μ F is not enough for the IG system to reach the reference voltage. An additional reactive current is required from the PWM converter (i_{di} >0). On the other hand, at higher per-unit speeds than 0.95 per-unit, the capacitor supplies more reactive current than that needed to reach the reference voltage, then the PWM converter has to supply inductive current (i_{di} < 0). At no-load, the converter active current becomes negligible. Thus, the PWM converter has to be dimensioned taking

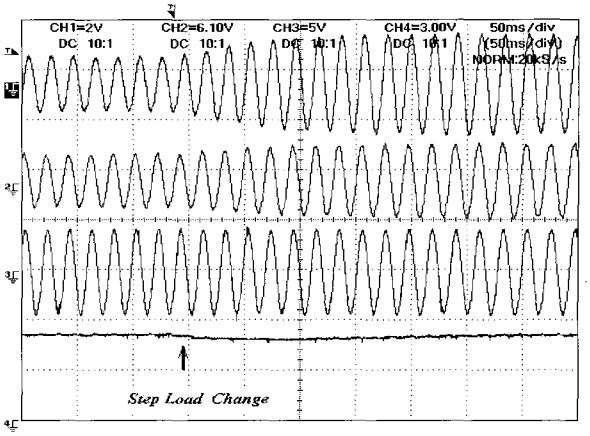

(1) Converter current -5A/div (2) IG current - 12.5A/div
(3) IG voltage -250V/div (4) DC link voltage -150V/div

Fig. 16 Measured operating waveforms of IG system

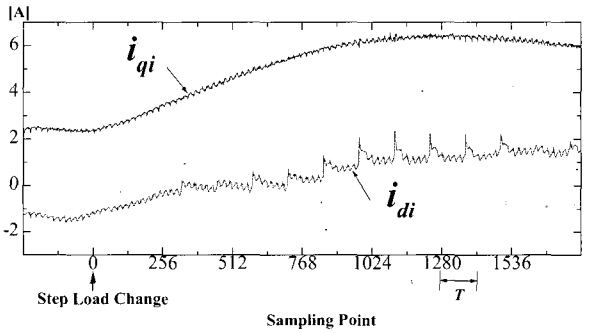

Fig. 17 *d-q* axis currents of PWM converter

into account the maximal reactive current only. Consequently, for a narrower operating speed range, a smaller converter size can be used. For example, if the speed range is between 0.9 per-unit and 1.0 per-unit value, the maximum inverter current will be only 10 % of the rated current of the IG.

4.3 IG and DC-Link Voltage Regulation with DC load

Several tests have been carried out to study the performances of the PWM converter in both transient and steady-state conditions, including bi-directional control of the reactive power flow with lagging, leading and a unity displacement factor. The DC-link voltage is regulated at 250 V while the line-to-line IG voltage is also regulated at 150V. Fig.16 shows the AC-side current of PWM converter, the IG current and line-to-line voltage and DC

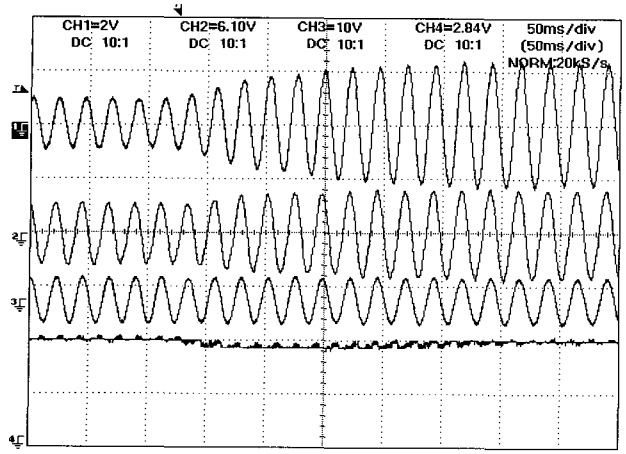

(1) Converter current -5A/div (2) IG current - 12.5A/div
(3) IG voltage -500V/div (4) DC link voltage -150V/div

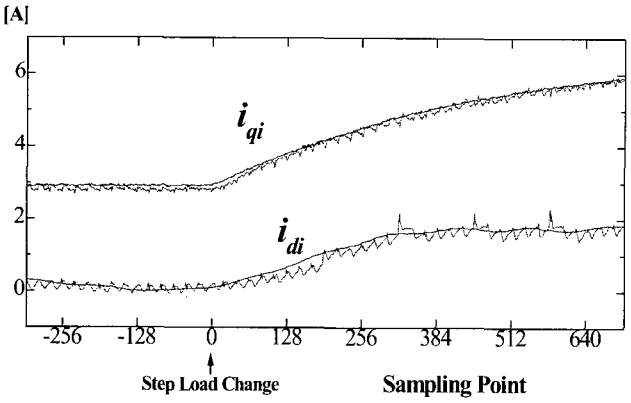

d-q axis currents of PWM converter

Fig. 18 Overall measured waveforms of IG system at n =1400 rpm

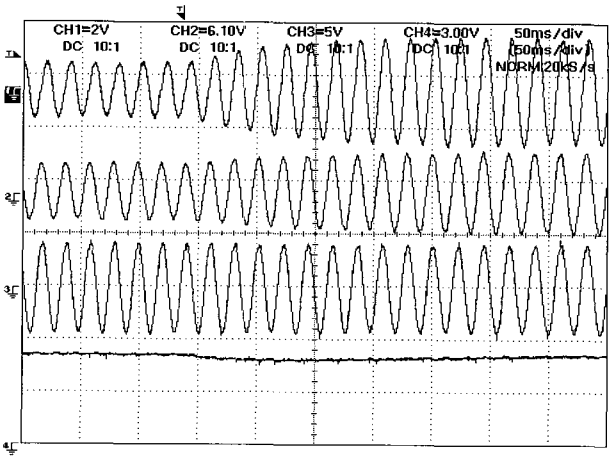

(1) Converter current -5A/div (2) IG current - 12.5A/div
(3) IG voltage -250V/div (4) DC link voltage -150V/div

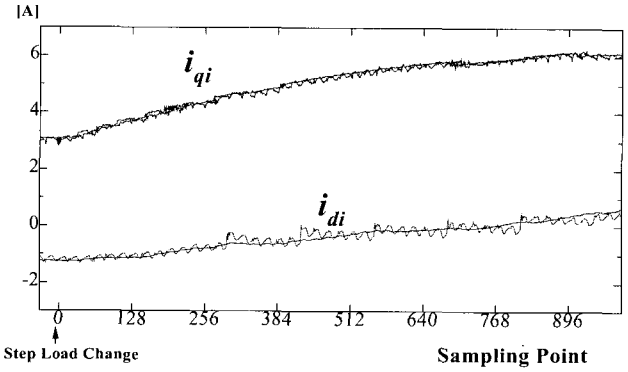

d-q axis currents of PWM converter

Fig. 19 Overall measured waveforms of IG system at n =1500 rpm

link voltage at a step change in the DC load power from 0.25 kW to 1 kW. This illustrates that the change in the overall operating waveforms of the proposed IG power conditioning system takes place within four cycles. These waveforms demonstrate the capability of the converter to control the DC link voltage and the IG output voltage by controlling the reactive power which depends on the speed of the prime mover to the IG or reactive power from the fixed capacitor used as a reactive power source for the stand-alone IG. This and a harmonics filter reduce the converter size. At the same time Fig.17 shows the response of the converter to the step change in DC load power. The reactive current demand is stepped from –1.3 A to + 1.5 A. Figs. 18, 19 and 20 show the waveforms demonstrating the capability of the PWM converter to control the DC link voltage and the IG output voltage with different speeds (1400rpm, 1500rpm, and 1600 rpm). The supplying reactive power to and from the IG generator depends on the value of the speed. The same performances can be observed for step changes in the AC load power with different speeds; the converter is also able to work at different speeds under these conditions. Fig.21 shows the ability of the IG power conditioning system to estimate the line-to-line voltage of the IG as compared to the measured value. Fig.22 proves the system is stable where the DC-link power is stepped from zero 0.25 kW to 1 kW and vice versa. As shown, the maximum error in the DC-link voltage is 12V(4.8 % of nominal) and recovery takes place within 150 ms, which is consistent with the control-loop design.

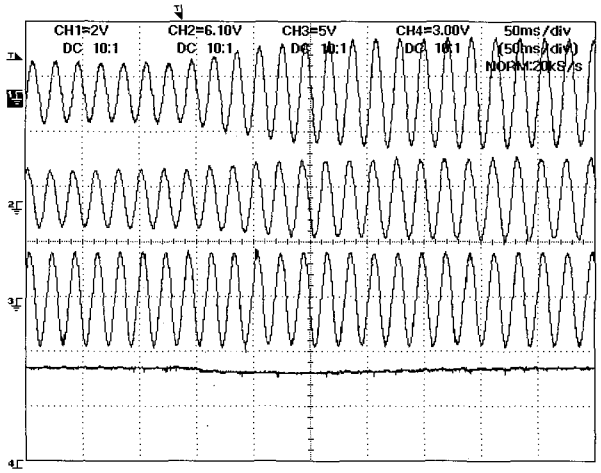

(1) Converter current -5A/div (2) IG current - 12.5A/div
(3) IG voltage -250V/div (4) DC link voltage -150V/div

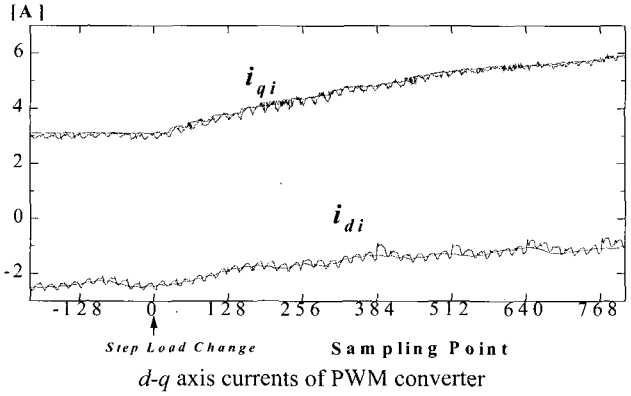

d-q axis currents of PWM converter

Fig. 20 Overall measured waveforms of IG system at n =1600 rpm

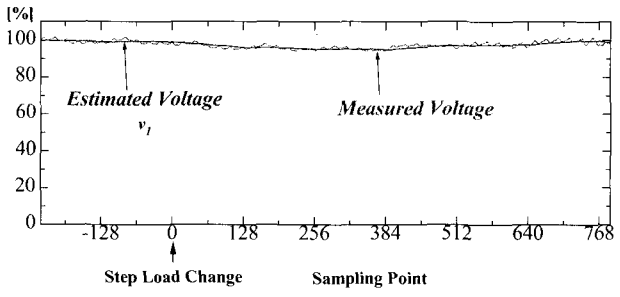

Fig. 21 Stator voltage of IG power conditioning system

5. Experimental Results with AC load

5.1 Operational waveforms to AC load variation

To reduce the system cost by continually reducing the size of the converter, the scheme depicted in Fig.1 is used

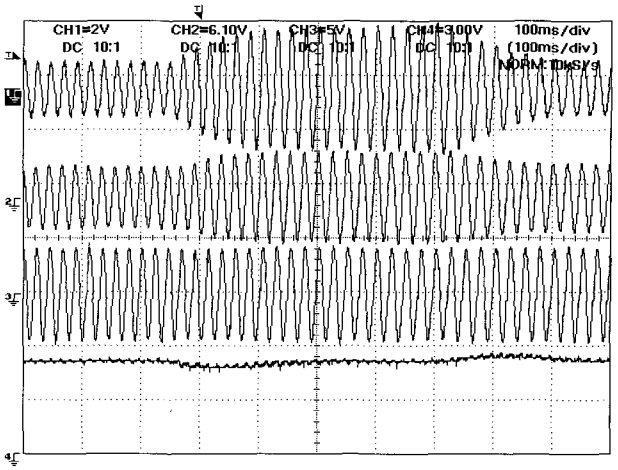

(1) Converter current -5A/div (2) IG current - 12.5A/div
(3) IG voltage -250V/div (4) DC link voltage -150V/div

Fig. 22 Measured waveforms of IG system at connecting /disconnecting load

while disconnecting the DC load from the DC-link side of the converter. The excitation to the induction machine (IM) is supplied by means of a PWM converter connected across the IM terminals via filter inductors. The rating of the converter is considerably less than the converter rating of the previous scheme with the DC load connected to the DC-link of the converter. In this case the converter with the fixed capacitor works to control the reactive power and needs very little active power to keep the DC-link voltage constant.

Several tests have been carried out to study the performances in both transient and steady-state conditions for a three-phase load only; resistive load as a heater in actual application causes the frequency of the IG to slightly change. A 2.2 kW, 220 V, 8.0 A, 60 Hz, 4-poles, squirrel-cage induction machine is used because the designed PWM converter has a smaller power rating compared to the previous one used with a 5 kW-IM machine. The equivalent-circuit parameters, L_{ls}=L_{lr}=3.57 mH, r_s=*0.9* Ω, and r_r=*0.9* Ω, are obtained by experimental measurements. The relationship between the magnetizing inductance L_m and the magnetizing phase current is obtained experimentally as depicted in Fig.23. The value of the magnetizing inductance L_m is a nonlinear function of a magnetizing phase current and may be expressed as follows:

$$L_m = \frac{1}{120\pi}\begin{Bmatrix} -0.1175\, i_m^5 + 1.918\, i_m^4 - 11.074\, i_m^3 \\ +25.387\, i_m^2 - 19.662\, i_m + 53.365 \end{Bmatrix} \quad (26)$$

With a fixed capacitor 100 μF, Fig.24 shows the measured waveforms of a three-phase load current, an AC-side current of a PWM converter, an IG current and an IG line-to-line voltage in the case of a three-phase load power stepped from 16 % to 50% at different prime mover speeds from 1300 rpm and 1550 rpm. The output voltage of the IG can be kept constant at 160 V, by adjusting the reactive component of the converter from a negative to positive value in accordance with the command of the IG voltage regulator. In the experiment at 1300 rpm, the converter current changed from -0.45 A to +0.55 A. Moreover, the DC-link voltage of the converter is also kept constant at 290V.

Fig. 25 and 26 show the overall operational waveforms at the steady-state operation of the IG system driven at speeds of 1300 rpm and 1550 rpm. In this case, the reactive component of the converter is controlled to cancell the voltage drop, caused by the increasing step of the active current, while the output frequency has been changed slightely from 42.9 Hz to 41.9 Hz at 1300 rpm and from 49.8 Hz to 49.1 Hz at 1550 rpm. Fig. 27 and 28. show the measured waveforms of the IG sysetm with a speed 1646 rpm and two different three-phase loads at 16 % and 50 % of the full load. The measured frequency has been changed from 54.127 Hz to 52.652 Hz

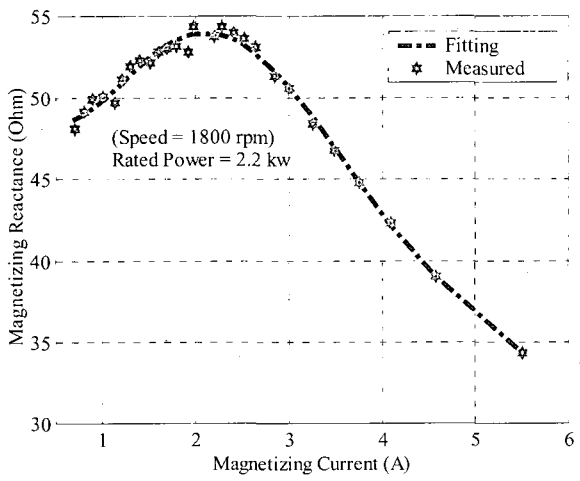

Fig. 23 Magnetizing curve, reactance versus current

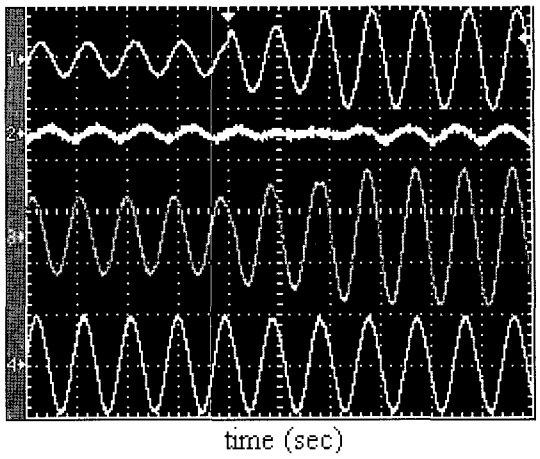

(a) speed , n =1300 rpm (42.9 Hz to 41.9 Hz), 25m sec /div

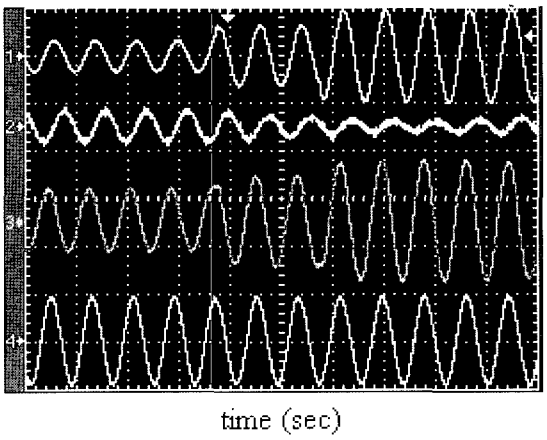

(b) n = 1550 rpm (49.8 Hz to 49.1 Hz), 25m sec /div

(1) AC load current -5A/div (2) Converter current -5A/div
(3) IG current – 5 A/div (4) IG voltage -250V/div,

Fig. 24 Measured waveforms of IG system with three-phase load power stepped from 16% to 50% of full-load power

5.2 IG system with AC load and speed variation

Fig. 29 shows the measured results of the proposed system to regulate the line-to-line voltage of IG within a wide speed range. IG voltage regulation can be automatically achieved with the speed variation of the PI controller which possesses the function of adjusting reactive current of the converter appropriately. In order to keep line-to-line voltage of the IG constant when the prime mover speed is increased, the reactive current of the IG consisting of the fixed capacitor, the three-phase load and converter currents, should be decreased. Fig.29 indicates that it is necessary to increase the inductive

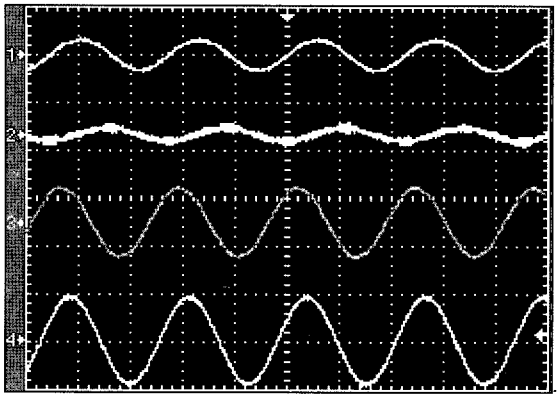

(a) speed , n =1300 rpm, 42.9 Hz, 10 m sec /div

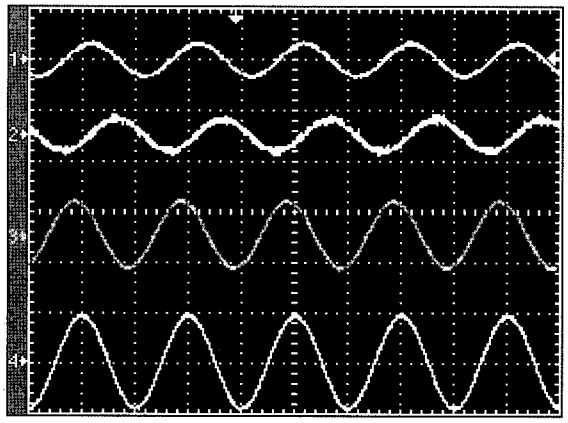

(b) n = 1550 rpm, 49.8 Hz , 10 m sec /div

(1) AC load current –2.5A/div (2) Converter current – 2.5A/div
(3) IG current – 2.5 A/div (4) IG voltage -250V/div.&

Fig. 25 Measured operating waveforms of IG system at steady-sate with 16 % of full-load power

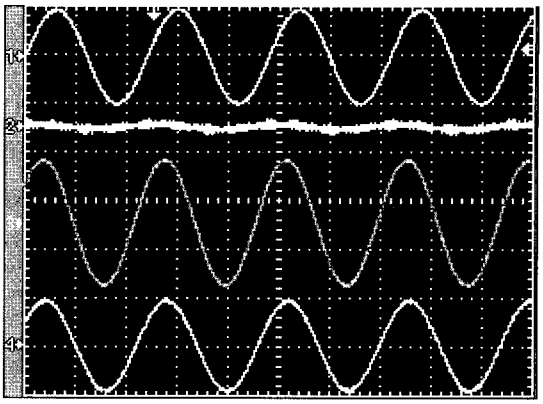

(a) speed , n =1300 rpm, 41.9 Hz, 10 m sec /div

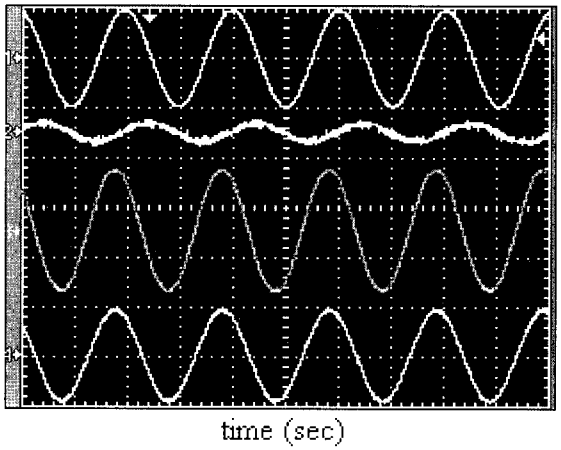

(b) n = 1550 rpm, 49.1 Hz, 10 m sec /div

(1) AC-load current -5A/div (2) Converter current -5A/div
(3) IG current – 5 A/div (4) IG voltage -250V/div.&

Fig. 26 Measured operating waveforms of IG system at steady-sate with 50 % of full-load power

reactive component of the converter when IG frequency is increased. The inductive reactive component of the converter should be made large enough to cancel the increment of capacitive current of the fixed capacitor because the total IG reactive current has to be decreased to maintain a constant IG voltage.

6. Conclusions

This paper has provided an advanced solution for wind turbine generators by applying an induction machine field oriented control and then describing the rotor field-oriented vector controlled induction generator for small-scale AC and DC power applications. The magnetization curve of the IG has been included in the proposed control system for improved accuracy in calculating the rotor flux position in spite of the control complexity. This is due to the fact that stable grid voltages are not available. Matlab/ Simulink environments supported the control and analysis for the IG excited by a capacitor bank and PWM converter and demonstrated that the voltage on the DC-link of a PWM converter and the terminals of the IG can be regulated within a wide range of change in three-phase loads and DC loads. Moreover,

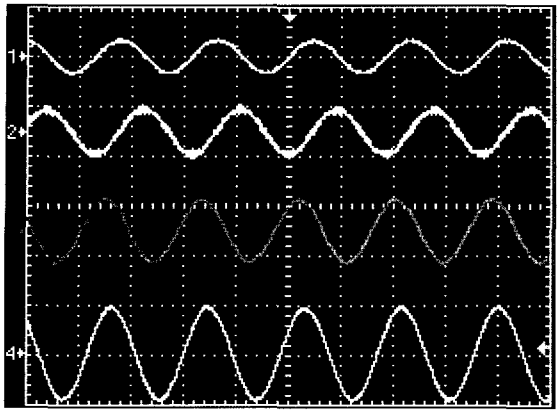

(1) AC-load current -5A/div (2) Converter current -5A/div
(3) IG current – 5 A/div (4) IG voltage -250V/div

Fig. 27 Measured waveforms of IG system at steady-sate with 16 % of full-load power, 1646 rpm and, 54.127 Hz

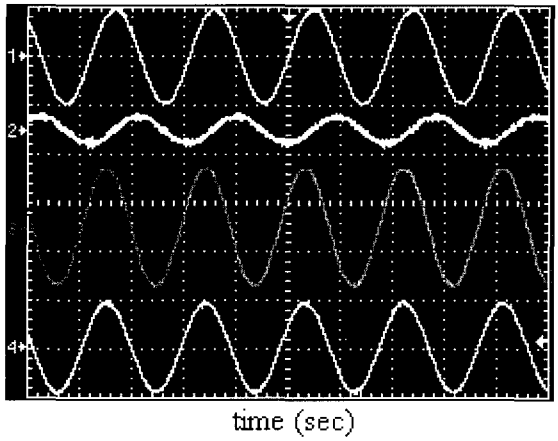

(1) AC-load current -5A/div (2) Converter current -5A/div
(3) IG current – 5 A/div (4) IG voltage -250V/div

Fig. 28 Measured waveforms of IG system at steady-sate with 50% of full-load power, 1646 rpm and 52.652 Hz

the proposed control system has provided a good voltage regulation for speeds above rated speeds and for speeds less than 0.9 per unit where the IG could show a good advantage in wind power application.

The proposed system was implemented as an output voltage control scheme for a stand-alone IG driven by a variable-speed prime mover and loaded by different independent three-phase and DC loading conditions. The variable-speed IG system has been shown to be well suited

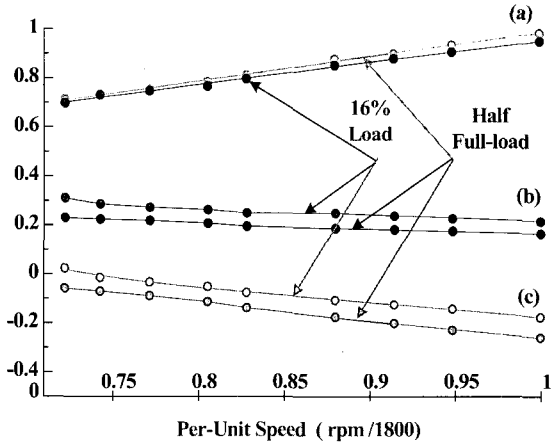

(a) Output Frequency of IG in per-unit,
(b) Reactive Current Component of IG in per-unit,
(c) Reactive Current Component of converter in per-unit

Fig. 29 Measured results of IG system at steady-sate with AC load power and different prime mover speeds

to wind power generation applications as a simple, rugged, low inertia, maintenance free, high reliability, simple control strategy and low cost AC and DC power source.

The major application of the stand-alone IG power system is in remote areas where utility lines are uneconomical to install. This system can be used for telecommunication, irrigation, and facilities in farms giving high conditions of comfort, reduction in the electric bills of companies or other large consumers and storage of energy during off-peak hours of consumption of the public network for reduction of the peak hours of larger demand. The stand-alone system must, therefore, have some means of storing energy, which can be used later to supply the load during the periods of low or no power output where the wind power outputs can fluctuate on an hourly or daily basis. Alternatively, the IG wind power system connected with 50Hz /60 /Hz can also be used in a hybrid configuration with a diesel engine generator in remote areas or fuel cells in urban areas.

Recently, alternative means of using this stand-alone system, whose frequency intrinsically varies over a modest range, has been investigated in addition to the energy storage opportunities created by storing energy in the form of hydrogen. This can be produced through advanced techniques involving the electrolysis of water and used for fuel cell power system.

References

[1] Alan and T. A. Lipo, "Control of a polyphase induction generator/induction motor power conversion system completely isolated from the utility," *IEEE Trans. Ind. Applicat.*, vol. 30, pp. 636–647, May/June 1994.

[2] T. Ahmed, O. Noro, E. Hiraki and M. Nakaoka, "Terminal Voltage Regulation Characteristics by Static VAR Compensator for a Three-Phase Self-Excited Induction Generator", IEEE Transactions on Industry Applications, Vol.40, No.4, pp.978–988, July-August 2004.

[3] R.C. Bansal, "Three-Phase Self-Excited Induction Generators: An Overview," IEEE Trans. on Energy Conversion, Vol.20, No.2 pp.292-299, June, 2005.

[4] E. Suarez and G. Bortolotto, "Voltage-Frequency Control of A Self-Excited Induction generator", IEEE Trans. on Energy Conversion, Vol.14, No.3 pp.394-401, September, 1999.

[5] E. Muljadi and T. A. Lipo, "Series compensated PWM inverter with battery supply applied to an isolated induction generator," *IEEE Trans. Ind. Applicat.*, vol. 30, pp. 1073–1082, July/Aug. 1994.

[6] E. G. Marra and J. A. Pomilio, "Self-excited induction generator controlled by a VS-PWM bidirectional converter for rural applications," *IEEE Trans. Ind. Applicat.*, vol. 35, pp. 877–883, July/Aug. 1999.

[7] O. Ojo and I. Davidson, "PWM-VSI inverter assisted stand-alone dual stator winding induction generator," in *Conf. Rec. IEEE-IAS Annu. Meeting*, Oct. 1999, pp. 1573–1580.

[8] T. Ahmed, K. Nishida and M. Nakaoka, "A Novel Induction Generator System for Small-Scale AC and DC Power Applications", Proceedings of the 36th Annual Power Electronics Specialists Conference, IEEE- PESC 05, Vol.1, pp.250 –256, 12-16 June 2005.

[9] M. Naidu and J. Walters, "A 4-kW 42-V Induction-Machine-Based Automotive Power Generation System With a Diode Bridge Rectifier and a PWM Inverter", IEEE Trans. on Industry Applications, Vol.39, No.5 pp.1287-1293, September/October, 2003.

[10] R. Leidhold, G. Garcia and M.I. Valla, "Induction generator Controller Based on the Instantaneous Reactive Power Theory", IEEE Trans. on Energy Conversion, Vol.17, No.3 pp.368-373, September, 2002.

Tarek Ahmed received his M.Sc. degree in electrical engineering from the Electrical Engineering Department, Faculty of Engineering, Assiut University, Egypt in 1998. He is an assistant lecturer in the Electrical Engineering Department, Faculty of Engineering, Assiut University, Assiut, Egypt. He is currently a Ph. D. candidate with the Power Electronic System and Control Engineering Laboratory in the Division of Electrical and Electronic Systems Engineering at the Graduate School of Science and Engineering, Yamaguchi University, Yamaguchi, Japan. He received Paper Awards from the Institute of Electrical Engineers of Japan (IEE-J) in 2003 and in 2004. His research interests are in the new applications of advanced high frequency resonant circuits and systems with renewable energy related soft switching PWM rectifiers and sine wave PWM inverter power conditioners. Mr. Ahmed is a student-member of the Institute of Electrical and Electronics Engineers of the USA (IEEE-USA), the Institute of Electrical Engineering and Installation of Engineers (IEIE-Japan), the Institute of Electrical Engineers (IEE-Japan) and the Japan Institute of Power Electronics (JIPE).

Katsumi Nishida received his B.S., and M.S. degrees in electrical engineering from the Tokyo Institute of Technology, Tokyo in 1976 and 1978, respectively. He received his Ph.D. degree from the Division of Electrical and Electronic Systems Engineering at the Graduate School of Science and Engineering, Yamaguchi University, Yamaguchi, Japan in 2002. He is engaged in research on power factor correction of PWM converters and current control of the three-phase active power filters using the dead-beat technique and the adaptive signal processing technique. Dr. Nishida is a member of the Institute of Electrical and Electronics Engineers of the USA (IEEE-USA), the Institute of Electrical Engineers of Japan (IEE-Japan) and the Japan Institute of Power Electronics (JIPE).

Mutsuo Nakaoka received his Dr.-Eng. degree in Electrical Engineering from Osaka University, Osaka, Japan in 1981. He joined the Electrical and Electronics Engineering Department of Kobe University, Kobe, Japan in 1981 and served as a professor of the Department of Electrical and Electronics Engineering at the Graduate School of Engineering, Kobe University, Kobe, Japan

until 1995. He is currently working as a professor in the Electrical and Electronics Engineering Department at the Graduate School of Science and Engineering, Yamaguchi University, Yamaguchi, Japan. His research interests include application developments of power electronics circuits and systems. He has received more than ten awards such as the 2001 premium prize paper award from IEE-UK, the 2001 and 2003 Best Paper Awards from IEEE-IECON, the 2000 third paper award from IEEE-PEDS, the 2003 James Melcher Prize Paper award from IEEE-IAS. He is now a chairman of the IEEE Industrial Electronics Society Japan Chapter. Dr. Nakaoka is a member of the Institute of Electrical Engineering Engineers of Japan, the Institute of Electronics, Information and Communication Engineers of Japan, the Institute of Illumination Engineering of Japan, the European Power Electronics Association, the Japan Institute of Power Electronics, the Japan Society of Solar Energy, the Korean Institute of Power Electronics, IEE-Korea and IEEE.